Optimal placement of battery swap stations in microgrids with micro pumped hydro storage systems, photovoltaic, wind and geothermal distributed generators

A. Rezaee Jordehi[a,1] , Mohammad Sadegh Javadi [2] , João P. S. Catalão [2,3]

[a]*Department of Electrical Engineering, Rasht Branch, Islamic Azad University, Rasht, Iran*

[2] *Center for power and energy systems, INESC TEC, Porto, Portugal*

[3]*Faculty of Engineering of University of Porto, Porto, Portugal*

Abstract

The penetration of electric vehicles (EVs) in vehicle markets is increasing; however long charging time in battery charging stations is an obstacle for larger adoption of EVs. In order to address this problem, battery swap stations (BSSs) have been introduced to exchange near-empty EV batteries with fully charged batteries. Refilling an EV in BSS takes only a few minutes. With decentralization of power systems, BSSs are typically connected to the microgrid (MG) in their neighborhood. Although the location of BSS in MG affects MG operation cost, to the best knowledge of the author, optimal placement of BSS has not been done from the perspective of MG. Therefore, in this paper, the objective is to find optimal location of BSSs in a MG with micro pumped hydro storage (PHS), photovoltaic, wind and geothermal units, while reactive power dispatch and all network constraints are considered by AC optimal power flow. The effect of BSS capacity and maximum charging/discharging power, BSS to MG link capacity, PHS capacity and maximum power of PHS unit on MG operation and optimal BSS location are investigated. DICOPT solver in general algebraic mathematical system (GAMS) is used to solve the formulated mixed-integer nonlinear optimisation problem.

Keywords: battery swap stations, microgrids, electric vehicles, energy management systems, energy

Nomenclature

[1]Corresponding author at: Rasht Branch, Islamic Azad University, Rasht, Iran. Tel: 981334404642; E-mail address: ahmadrezaeejordehi@gmail.com. The source codes may be requested by Email to the corresponding author.

Indices

t	Index of time
i, m	Indices of buses
j	Index of thermal DGs
pv	Index of PV units
w	Index of wind units
gt	Index of geothermal units
bss	Index of BSS units
phs	Index of PHS units

Sets

S	Set of buses
U	Set of buses with PHS units
B_i	Set of buses connected to bus i
G	Set of thermal DGs
G_i	Set of thermal DGs connected to bus i
BR	Set of branches
BR_i	Set of branches connected to bus i

Parameters

Δt	Operation resolution
v_i	Status of connection of bus i to point of common coupling (PCC)
bid	Bid of thermal DGs for real power
RU/RD	Ramp-up/down rate limit of thermal DGs
P_{min}/P_{max}	Minimum/maximum active power of thermal DGs
Q_{min}/Q_{max}	Minimum/maximum reactive power of thermal DGs
$size_{bss}$	Size of BSS
N_{bss}	Number of BSSs
$E_{bss,ini}$	Initial energy level of BSS
$E_{bss,min}$	Minimum allowed energy level of BSS
$E_{bss,max}$	Maximum allowed energy level of BSS

$P_{bss,max}$ Maximum allowable power flow between BSS and MG

$P_{it,avail}^{w}$ Available wind power at bus i and time t

$P_{it,avail}^{pv}$ Available PV power at bus i and time t

$P_{it,avail}^{gt}$ Available geothermal power at bus i and time t

ρ_t Market price at PCC at time t

$P_{grid,max}$ Power flow capacity of the link between MG and grid

P_{it}^{D}/Q_{it}^{D} Active/reactive power demand at bus i and time t

$Z_{im}\measuredangle\alpha_{im}$ Phasor of series impedance of branch between buses i and m

B_{im} Susceptance of branch between buses i and m

$Slim_{im}$ Apparent power flow limit of branch between bus i and bus m

V_{min}/V_{max} Minimum/maximum allowable voltage magnitude of buses

$Pshed_{i,max}$ Maximum real power at bus i that may be shed

$VOLL_t$ Value of loss of load at time t

$E_{phs,i,ini}$ Initial energy level of PHS at bus i

$E_{phs,i,final}$ Energy level of PHS at bus i at the end of scheduling horizon

$E_{phs,i,min}/E_{phs,i,max}$ Minimum/maximum allowed energy level of PHS at bus i

Variables

u_i Availability of BSS at bus i

Pf_{imt}/Qf_{imt} Real/reactive power flow of branch between bus i and bus m at time t

S_{imt} Apparent power of branch between bus i and bus m at time t

P_{jt}/Q_{jt} Real/reactive power generated by jth thermal DG at time t

$P_{grid,t}$ Power exchange between MG and grid

$Pshed_{it}$ Power not supplied at bus i and time t

$E_{phs,it}$ Energy level of PHS unit at bus i and time t

$P_{phs,it}$ Charging/discharging power of PHS unit at bus i and time t

$P_{bss,it}$ Power absorbed by BSS from MG at bus i and time t

$E_{bss,it}$ BSS energy level at bus i and time t

P_{it}^{w} Dispatched wind power at bus i and time t

P_{it}^{pv} Dispatched PV power at bus i and time t

P_{it}^{gt} Dispatched geothermal power at bus i and time t

OP Operation cost of MG

OF Planning cost

INV Investment cost of BSS

$V\measuredangle\delta$ Voltage phasor of buses

1. Introduction

Microgrids (MGs) have been developed to enable optimal utilisation of distributed energy resources (DERs). MG is a cluster of distributed generation (DG) units, energy storage systems and loads that as a single controllable entity can operate either autonomously or connected to an upstream grid [1]. In remote areas where power grids are not accessible, isolated MGs may be set up to feed local demand and in areas that power grid is accessible, MGs are connected to the grid and utilise power exchange capability with grid to minimise their operation cost [2-4]. Thanks to high penetration of renewable energy resources, MGs are more environmental friendly than conventional grids and typically offer higher reliability than conventional grids [5, 6].

Transportation is a sector that emits a large portion of greenhouse gases and uses a lot of fossil fuels [7-9]. Transportation electrification was a revolution aimed to decrease the emission of greenhouse gases and also decrease the reliance on fossil fuels. The penetration of electric vehicles (EVs) is increasing; however the long charging time of EVs in battery charging stations (BCSs) is a barrier for their larger adoption [10]. In order to address this problem, battery swap stations (BSSs) were introduced to exchange near-empty EV batteries with fully charged batteries [10]. Refilling an EV in BSS takes only a few minutes and is not longer than refilling conventional vehicles in fuel stations. EVs that use BSSs do not purchase batteries, but batteries are leased to them, so the EV sticker price is decreased [11]. Lithium Ion is the most commonly used battery in EVs [12].

BSSs charge their batteries either with their own renewable power resources such as PV and wind resources or through a power grid/MG. In the latter case, they have the capability of power exchange with grid/MG. BSSs are able to charge their stocked batteries at low-price times. They offer advantages to power grids/MGs; through their battery to grid (B2G) capability, BSSs decrease operation cost of grid/MG, moreover, they can provide spinning reserve for grids/MGs [10]. An important point is that the location of BSS in a power system may affect power system operation cost and finding its optimal location is crucial, however this issue has been rarely addressed in the literature.

In [12], differential evolution (DE) with fitness sharing strategy has been used for optimal placement and sizing of BSSs from perspective of BSS owner, while the security constraints of power system are also considered. BSS planning problem has been formulated as a non-convex mixed-integer nonlinear programming (MINLP) and net present value (NPV) of the BSS project is minimised considering life cycle cost criterion. The penetration rate of EVs over time has been modeled as a geometric Brownian motion function and Monte Carlo Simulation (MCS) has been used for dealing with uncertainties. The results show that BSS causes a flatter demand profile for power system, while battery charging stations (BCSs) develop new peaks in demand profile.

In [13], grasshopper optimisation algorithm has been used to find optimal location and size of BSSs in power systems. Planning problem has been formulated as a multi-objective optimisation problem, while the objectives are energy loss and voltage stability, however the changes of electricity price over time has not been considered. Linear weighted sum (LWS) has been used for transforming the multi-objective optimisation problem into a single-objective optimisation problem. In order to facilitate charging of EVs in BSSs, power system has been sectionalized into multiple zones. The results show that grasshopper optimisation algorithm performs better than particle swarm optimisation (PSO), gravitational search algorithm and artificial bee colony. In [14], the route and BSS location are determined for a fleet of EVs so that investment cost of BSSs and shipment cost of EVs are minimised. The emission of EVs is to deliver goods to customers at different nodes. Each customer must be visited by one and only one EV. CPLEX as a mixed-integer programming (MIP) solver and Tabu search are used for solving the formulated optimisation problem.

Nowadays, with decentralization of power systems and increase in the number of MGs, BSSs are commonly connected to the MG in their neighborhood. Considering the reviewed literature, to the best knowledge of the author, optimal placement of BSS in MGs has not been done from the perspective of MG. Therefore, in this paper, the objective is to find optimal location of BSSs in a MG with micro PHS unit, photovoltaic (PV), wind and geothermal DG units, while all network constraints and reactive power dispatch are considered. It is assumed that all facilities except for thermal DGs are owned by MG owner and the optimisation is done from MG perspective. DICOPT solver in general algebraic mathematical system (GAMS) has been used for solving the formulated mixed-integer nonlinear optimisation problem [15, 16]. The contributions of the paper are listed out as below.

- ✓ Optimal placement of BSSs in MGs is done from perspective of MG.
- ✓ Micro PHS unit as an energy storage system (ESS) and PV, wind and geothermal power units are used in the MG.
- ✓ AC optimal power flow is done and all network constraints are satisfied.

- ✓ The effect of BSS capacity, BSS to MG link capacity, micro PHS unit capacity and maximum power of micro PHS unit on MG operation are investigated.

The case study is a MG with two PV units, two wind units, two geothermal units, one micro PHS unit and one BSS. The rest of the paper is organised as follows; in section 2, the performance of renewable components of the MG and PHS units are explained. In section 3, optimal placement of BSS in MGs with PHS, PV, wind and geothermal units is formulated as a MINLP. The results and analysis of results can be found in section 4. Finally, section 5 contains the conclusions of the paper.

2. MG components

In this section, the components of the MG studied in this paper are introduced. Small-scale wind and PV units are renewable and sustainable energy resources that are commonly used in MGs. In wind generation units, wind energy is used to turn turbines of distributed generators and in PV units, PV cells directly convert sunlight into electric power. Both wind and PV units represent volatile and intermittent sources of power and thanks to technological advances, have reached grid parity in very regions of the world [17, 18]. Their lifecycle emissions is low [19, 20].

Geothermal power is very scalable and small-scale to large-scale geothermal units may be used in MGs [21]. In geothermal power units, using fluid circulation methods such as magma conduits, oil wells and hot springs, the heat of earth is carried to the surface and used to heat working fluid that must turn the turbine of generator [22, 23]. It is a renewable and sustainable power resource as the heat absorbed by geothermal power plants from earth is negligible in comparison with earth heat content [24]. The greenhouse gas emission of geothermal power units is less than 5% of fossil fuel-based generators [25]. It is envisioned that by 2050, geothermal power would supply 3-5% of global electricity demand [26].

There are diverse forms of energy storage systems [27, 28]. PHS system is considered as a well-established technology for large-scale electricity storage and consist of two water reservoirs in different altitudes connected via a penstock [29]. Typically, during low demand time periods, water is pumped to the higher basin and during peak times the water is released to the lower basin and the released energy turns hydro-turbine and generates electricity [29]. PHS systems as other energy storage systems may mitigate the volatility of renewable power resources in MGs and decrease their operation cost. They also enhance voltage and frequency stability of MGs and decrease the shadow prices.

3. Problem formulation

The model for planning BSSs in a grid-connected MG with PHS, PV, wind, geothermal and thermal DGs is characterised by (1)-(28). This is a MINLP model, wherein the planning cost as the sum of BSS investment cost and MG operation cost is minimised. MG operation cost consists of the cost of power purchased from thermal DGs, cost of power imported from upstream grid and cost of load shedding is minimised. **Operation cost of PV, wind and geothermal units is assumed zero.**

$$OF = INV + OP \qquad (1)$$

$$OP = \sum_{t}\sum_{j} bid_{jt}P_{jt}\Delta t + \sum_{t} P_{grid,t}.\rho_t\Delta t + \sum_{i}\sum_{t} Pshed_{it}.VOLL_{it}\Delta t \qquad (2)$$

Power flow equations are represented as (3)-(6). Equation (3) ensures that at each bus of the MG and at each time, sum of power of thermal DGs, power of PV, wind and geothermal DGs, power not served to consumers, discharging power of PHS and BSS to MG power matches the sum of active power demand at that bus, charging power of PHS at that bus and power flowing out from that bus to other buses. Charging power of PHS is the electric power consumed to pump water to the higher basin and its discharging power is the generated electric power when water is released to the lower basin.

Reactive power balance equations at MG buses are represented by (4).

$$\sum_{j\epsilon G_i} P_{jt} + Pshed_{it} + P_{it}^{w} + P_{it}^{pv} + P_{it}^{gt} - P_{it}^{D} - P_{phs,it} - u_i P_{bss,it} + v_i P_{grid,t} = \sum_{m\epsilon B_i} Pf_{imt} \quad \forall i, \forall t \qquad (3)$$

$$\sum_{j\epsilon G_i} Q_{jt} - Q_{it}^{D} = \sum_{m\epsilon B_i} Qf_{imt} \quad \forall i, \forall t \qquad (4)$$

$$Pf_{imt} = \frac{V_{it}^2 \cos(\alpha_{im})}{Z_{im}} - \frac{V_{it}.V_{mt}}{Z_{im}} \cos(\delta_{it} - \delta_{mt} + \alpha_{im}) \quad \forall i, \forall m \in B_i, \forall t \qquad (5)$$

$$Qf_{imt} = \frac{V_{it}^2 \sin(\alpha_{im})}{Z_{im}} - \frac{V_{it}.V_{mt}}{Z_{im}} \sin(\delta_{it} - \delta_{mt} + \alpha_{im}) - \frac{B_{im}}{2} V_{it}^2 \quad \forall i, \forall m \in B_i, \forall t \qquad (6)$$

Voltage magnitude of buses and apparent power of branches in the MG are limited by constraints (7) and (8) and power exchange between MG and grid is limited by (9). This set of constraints is imposed due to thermal limit of the line and transformer connecting MG and grid. For each thermal DG, as represented by (10)-(11),

real power and reactive power are confined within a pre-specified range and the rapid changes in its real power is not allowed by (12)-(13). Equations (14) are imposed to ensure that at each bus and each time, the shed power does not exceed a pre-specified limit.

$$V_{min,i} \leq V_{it} \leq V_{max,i} \qquad \forall i, \forall t \qquad (7)$$

$$\sqrt{\left(Pf_{imt}^{2} + Qf_{imt}^{2}\right)} \leq Slim_{im} \qquad \forall i, \forall m \in B_i, \forall t \qquad (8)$$

$$-P_{grid,max} \leq P_{grid,t} \leq P_{grid,max} \qquad \forall t \qquad (9)$$

$$P_{min,j} \leq P_{jt} \leq P_{max,j} \qquad \forall j, \forall t \qquad (10)$$

$$Q_{min,j} \leq Q_{jt} \leq Q_{max,j} \qquad \forall j, \forall t \qquad (11)$$

$$\boldsymbol{P_{jt} - P_{j(t-1)} \leq RU_j \, \Delta t} \qquad \boldsymbol{\forall g, \forall t \neq 1} \qquad \boldsymbol{(12)}$$

$$\boldsymbol{P_{j(t-1)} - P_{jt} \leq RD_j \, \Delta t} \qquad \boldsymbol{\forall g, \forall t \neq 24} \qquad \boldsymbol{(13)}$$

$$0 \leq Pshed_{it} \leq Pshed_{i,max} \qquad \forall i, \forall t \qquad (14)$$

The operation of PHS is subject to constraints (15)-(19). When ith PHS is pumping water to the upper basin, $P_{phs,it}$ is positive and when it is releasing the energy of water and injects power to the MG, $P_{phs,it}$ is negative. As per (15)-(16), the energy level of PHS at each time is equal to its energy level at previous time plus the energy it absorbs from MG/minus the energy it injects to MG (depending on its operation mode). Constraints (16) apply to the first time period of operation horizon and constraints (15) apply to the other time periods.

Constraints (17) and (18) are respectively imposed to confine energy level and charging/discharging power of PHS. Equation (19) ensures that the energy level of PHS at the beginning of scheduling horizon equals its energy level at the end of the scheduling horizon.

$$\boldsymbol{E_{phs,it} = E_{phs,i(t-1)} + P_{phs,it} \, \Delta t \quad \forall i \in U} \qquad \boldsymbol{(15)}$$

$$\boldsymbol{E_{phs,it} = E_{phs,i,ini} + P_{phs,it} \, \Delta t \quad \forall i \in U} \qquad \boldsymbol{(16)}$$

$$E_{phs,i,min} \leq E_{phs,it} \leq E_{phs,i,max} \qquad \forall i \qquad (17)$$

$$-P_{phs,i,max} \leq P_{phs,it} \leq P_{phs,i,max} \qquad \forall i, \forall t \qquad (18)$$

$$E_{phs,i,ini} = E_{phs,i,final} \qquad (19)$$

The operation of BSS is subject to constraints (20)-(25). Constraint (20) ensures that for each BSS, at the end of scheduling horizon, all empty EV batteries are fully charged. As per (21)-(22), the energy of BSS at each time is

equal to its energy at previous time plus power that is flowing into BSS. Constraints (22) apply to the first time period of operation horizon and constraints (21) apply to the other time periods. Equation (23) ensures that energy level of no BSS falls within a pre-specified range and constraints (24) are imposed to confine power flow between MG and BSS. **Constraint (25) is imposed to ensure that the desired number of BSSs is placed in the MG.**

$$\sum_t P_{bss,it}\Delta t = u_i\, size_{bss} \quad \forall i \qquad (20)$$

$$E_{bss,it} = E_{bss,i(t-1)} + P_{bss,it}\Delta t \quad \forall i \qquad (21)$$

$$E_{bss,it} = E_{bss,,i,ini} + P_{bss,it}\Delta t \quad \forall i \qquad (22)$$

$$E_{bss,i,min} \le E_{bss,it} \le E_{bss,i,max} \quad \forall i \qquad (23)$$

$$-P_{bss,i,max}u_i \le P_{bss,it} \le P_{bss,i,max}\, u_i \quad \forall i, \forall t \quad (24)$$

$$\sum_i u_i = N_{bss} \qquad (25)$$

Eventually, the operation of PV, wind and geothermal units are subject to the following constraints.

$$0 \le P_{it}^{w} \le P_{it,avail}^{w} \qquad (26)$$

$$0 \le P_{it}^{pv} \le P_{it,avail}^{pv} \qquad (27)$$

$$0 \le P_{it}^{gt} \le P_{it,avail}^{gt} \qquad (28)$$

4. Results and analysis

A MG with 33 buses, 32 branches, 4 thermal DGs, 2 PV units, 2 wind units, 2 geothermal power units and one PHS unit has been used as the case study. Since the objective is to find optimal location of BSSs with known size and investment cost is constant, the best plan would be the one minimising daily operation cost of the MG. Bus and branch data of the MG is available in [30] and its single line diagram can be seen as Fig.1. Data of thermal DGs can be found in Table 1. Table 2 contains capacity and location of PV, wind, geothermal power and PHS unit and time factors of demand, PV and wind generation and market price at PCC can be found in Table 3. BSS is supposed to serve 400 Tesla 3 EVs with 75 kWh batteries per day. So, BSS capacity is 30000 kWh. Maximum power exchange between BSS and MG has been assumed 1.5 pu and initial energy level of both BSS and PHS is equal to zero. Maximum energy level of PHS is 5000 kWh, its maximum charging and maximum discharging power are 0.50 pu and maximum power exchange between MG and grid is 2 MW.

Minimum and maximum allowable voltage of buses are respectively 0.9 pu and 1.1 pu. Base apparent power is 1000 kVA and base voltage is 12.66 kV. At the beginning of the operation horizon, energy level of both BSS and PHS are equal to zero. Scheduling horizon is 24 hours and scheduling resolution is 1 hour.

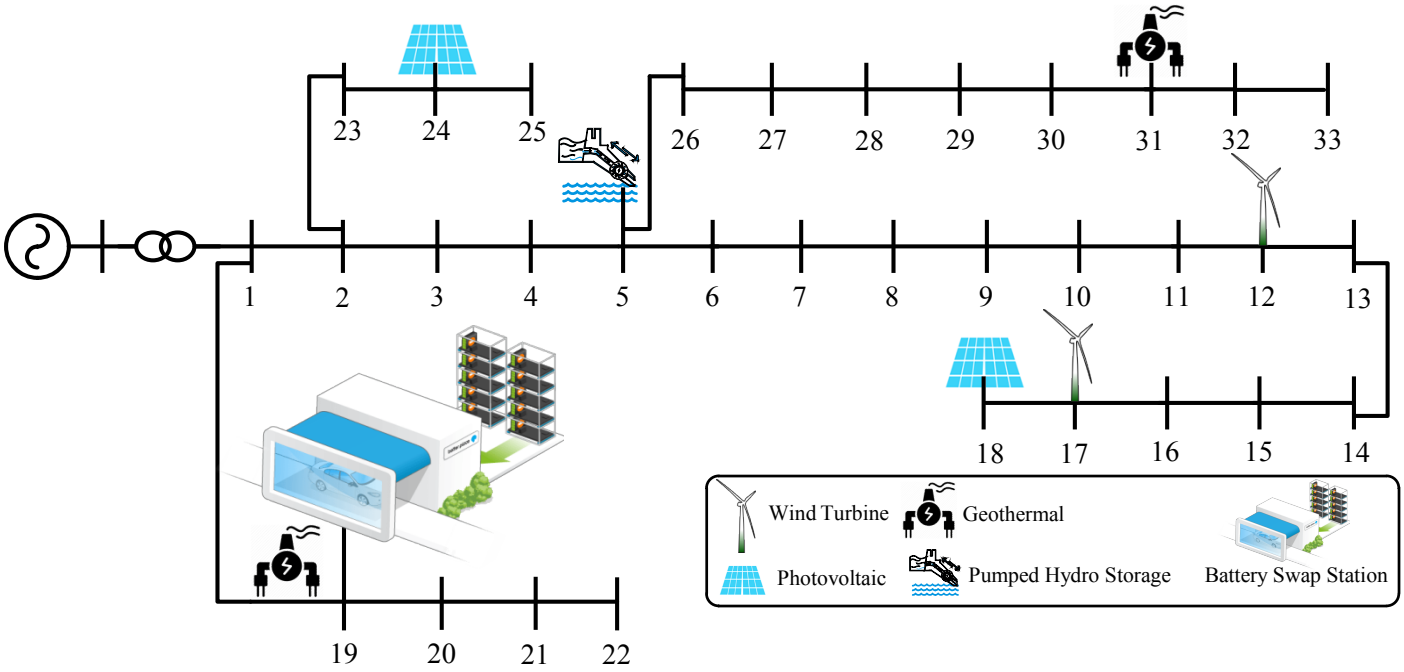

Fig.1. Single line diagram of the studied MG

Table 1. Data of thermal DGs

Connected bus number	Minimum active power (kW)	Maximum active power (kW)	Minimum reactive power (kVAr)	Maximum reactive power (kVAr)	Bid($/kWh)	Ramp up limit (kW/h)	Ramp down limit (kW/h)
2	300	2500	0	1000	0.154	500	500
11	300	1000	0	1000	0.157	400	400
15	200	1000	0	500	0.218	300	300
27	200	1000	0	300	0.194	300	300

Table 2. Capacity and location of PV, wind, geothermal power and PHS units

Unit	Connected bus	Capacity
PV #1	18	400 kW
PV #2	24	500 kW
Wind #1	12	500 kW
Wind #2	17	350 kW
Geothermal #1	19	1000 kW
Geothermal #2	31	500 kW
PHS	5	5000 kWh

Table 3. Time factors of demand, PV and wind generation and market price at PCC

Hour	Demand [31]	PV [32]	Wind [16]	Market price at PCC ($/kWh) [33]
1	0.800	0	0.07867	0.230
2	0.805	0	0.08667	0.190
3	0.810	0	0.11733	0.140
4	0.818	0	0.25866	0.120
5	0.830	0.02	0.36133	0.120
6	0.910	0.1080	0.56667	0.130
7	0.950	0.2790	0.65066	0.130
8	0.970	0.5190	0.56666	0.140
9	1.000	0.7424	0.4840	0.170
10	0.980	0.9184	0.5480	0.220
11	1.000	0.9755	0.75733	0.220
12	0.970	0.9678	0.71066	0.220
13	0.950	1.0000	0.87066	0.210
14	0.900	0.9040	0.93200	0.220
15	0.905	0.8105	0.96667	0.190
16	0.910	0.6980	1.000	0.180
17	0.930	0.4675	0.86933	0.170
18	0.900	0.2520	0.66533	0.230
19	0.940	0.0940	0.65600	0.210
20	0.970	0.0200	0.56133	0.220
21	1.000	0.0010	0.56533	0.180
22	0.930	0	0.55600	0.170
23	0.900	0	0.72400	0.130
24	0.940	0	0.84000	0.120

DICOPT solver in GAMS has been used for solving the proposed MINLP model. Different aspects of the model are investigated in different subsections of this section; in subsection 1, optimal power flow in the MG is done with optimal placement of BSS(s). In subsection 2, sensitivity of MG operation with respect to BSS location as well as effect of BSS capacity and BSS-MG power exchange limit on MG operation and optimal BSS location is investigated. In subsection 3, the effect of PHS unit, effect of PHS capacity and maximum PHS power on MG operation cost and optimal BSS location is investigated.

4.1. Optimal power flow in MG with optimal placement of BSS

In this subsection, optimal power flow is done in the MG with optimal placement of BSS(s). With one BSS, operation cost of the MG is $9689.4629 and bus #19 is the optimal location of BSS. Placing BSS at bus #19 results in such voltages, power flows and losses that minimises MG operation cost. Due to very high value of lost load, load shed at all buses and all times is equal to zero. Fig.2 shows BSS power at different times and indicates that in order to impose the least operation cost to the MG, at hours such as 2-9, 15-17 and 21-24, when market price at PCC and locational marginal prices (LMPs) are low, BSS is charged with maximum power. At the end of the scheduling horizon, BSS energy level is 30000 kWh; that is, all batteries are fully charged. Fig.2 also shows that at hours 2-9, 15-17 and 21-24 maximum charging power of BSS is binding.

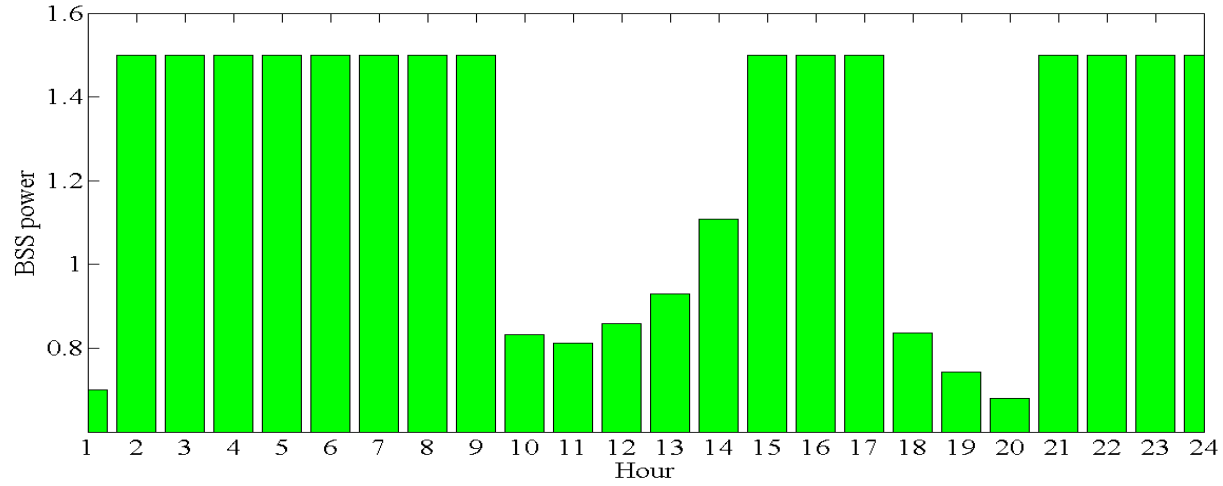

Fig.2. BSS schedule

Fig.3 shows power of PHS at different times and indicates that at hours 3-9 with low prices at PCC and low LMPs, PHS is charged, then it is discharged at high-price hours 10-15 to inject discharging power to the MG and increase MG energy arbitrage capability. Again, at low-price hours 16-17, it is charged and then discharged at high-price hours 18-20 to increase export capability and benefit of MG. Fig.3 also shows that at most of the times, power limit of PHS is a binding constraint, while maximum energy constraint of the MG is not binding at any time.

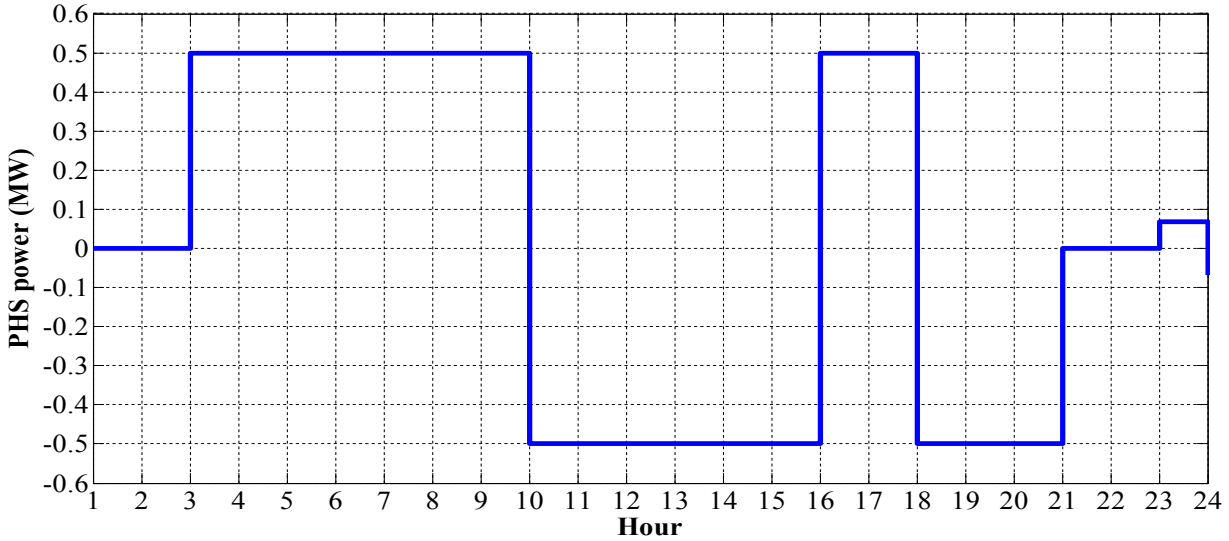

Fig.3. Power of PHS unit

Fig.4 includes schedule of DERs and power exchange of MG and grid at different times. Fig.5 shows reactive power of DERs and Fig.6 shows the variations of shadow prices over time. According to table 3 and Fig.4, it is inferred that the dispatch of DERs in MG mainly depends on MG demand level, bids of DGs and market price

at PCC. At hour 1, market price at PCC is at its maximum value, i.e., 230 $/MWh, so MG operator uses this opportunity to make a profit by loading its cheaper DGs and export the extra power to the grid. At this time, as per power exchange limit between MG and grid and demand level, for full utilisation of energy arbitrage capability, it is enough to fully load DG1, DG2 and DG4. Due to ramp-down rate limit, DG4 cannot generate more than 500 kW, therefore DG1 and DG2 are fully loaded, DG4 generates 500 kW and DG3 as the most expensive energy resource is loaded with its minimum power, i.e., 200 kW. Power generated by these thermal DGs plus the power generated by PV, wind and geothermal power units supply MG demand, 2 MW of extra power is exported to the grid and the remaining 0.7011 MW is used to charge BSS batteries. Actually, at this time charging BSS or PHS with DG3 is not economical as it is an expensive power resource, so PHS is in idle mode. At this time, power exchange limit with grid and upper power limits of DG1 and DG2 are binding constraints; that is with higher values for their limits, MG operation cost could be lowered.

At hour 2, market price at PCC decreases and gets less than bids of DG3 and DG4. At this condition, it seems rational for MG to load DG1 and DG2 as the cheaper power resources with maximum power and export the extra power to the grid. However, fully loading DG1 at this hour imposes a considerable cost to the MG at the next hour. If at this hour, DG1 is fully loaded, at next hour when market price at PCC is very low and power of DG1 must be decreased, due to ramp-down rate limit, it would be obliged to generate at least 2 MW and this imposes considerable additional cost to the MG. Therefore, DG1 is loaded with 2 MW, DG2 is fully loaded and DG3 and DG4 are loaded with minimum power, 2.9906 MW demand of MG is fed, BSS is charged with its maximum power, i.e., 1.5 MW and the extra 387.5 kW is exported to the grid. At this time, it is not economical to charge PHS instead of exporting power to the grid and PHS is still in its idle mode.

At hour 3 market price at PCC decreases further and gets lower than bid of all DGs, so the maximum possible power must be imported from grid. This condition persists until the end of hour 8. These hours with cheap grid power prices are right times to charge BSS and PHS. As Fig.3 and Fig.4 show, at hours 3-8, both BSS and PHS are charged with their maximum charging power. At all these times, DG3 and DG4 are loaded with minimum power. Due to ramp-down rate limits, power of DG1 cannot fall respectively below 1.5 MW and 1 MW at hours 3 and 4 and power of DG2 is not allowed to fall below 0.6 MW at hour 3. At hour 6, since voltage limits are binding constraints, DG1 as the cheapest DG is not fully load, while DG2 as the more expensive DG is loaded with more than its minimum power. At hours 5-7, the limit of power exchange between MG and grid is a binding constraint; that is, a lower MG operation cost could be achieved with higher power exchange limit.

At hour 9, DG1 and DG2 are cheaper power resources than grid, so they are loaded with maximum possible power. Due to ramp-up rate limits, at this time, maximum possible power for DG1 and DG2 are respectively 2.0636 MW and 0.8468 MW. At this time, 0.5721 MW is imported from grid and BSS and PHS are charged

with their maximum charging power. Grid is the marginal power resource and sets marginal price as 170 $/MWh. At hour 10 market price at PCC increases and for hours 10-14, it is high, so at this time period, MG purchases power from cheaper DGs and discharges PHS to supply demand, charge BSS and export the extra power to grid. For instance, at hour 10, DG1 and DG2 are fully loaded and DG4 as the marginal generator is partially loaded and sets marginal price. See locational marginal price at this hour for bus 1 which is 195.9 $/MWh and is very close to bid of DG4 (194 $/MWh). The small difference between LMP at bus 1 and bid of DG4 is due to power loss in branches.

At hours 15-17, market price at PCC is lower than bids of DG1 and DG2, but higher than bids of DG3 and DG4, so DG1 and DG2 are fully loaded and DG3 and DG4 are loaded with minimum power and BSS is charged with maximum power. At hour 15 when market price at PCC is higher than the next two hours, PHS is discharged to decrease MG operation cost, but it is charged at the next two hours.

At hours 18-20, market price at PCC is high, so it is the right time to discharge PHS and load thermal DGs with maximum possible power to make profit through export of maximum possible power to the grid. At these hours, DG4 is the marginal generator and sets LMP. At hours 21-22, when DG1 and DG2 bid cheaper than grid power, grid serves as marginal generation resource and sets LMP and BSS is charged with maximum charging power. Eventually, at hours 23 and 24 when market price is very low and lower than bids of all thermal DGs, thermal DGs are loaded with the least possible power and the required power is mostly supplied by grid. Due to ramp-down rate limit, power of DG1 is gradually decreased from 1.5 MW at hour 22 to 1 MW at hour 23 and 0.5 MW at hour 24. With cheap grid power, BSS is charged at hours 23 and 24. PHS is also charged with cheap grid power in hour 23, however in order to equalize its initial and final energy, it is discharged at hour 24.

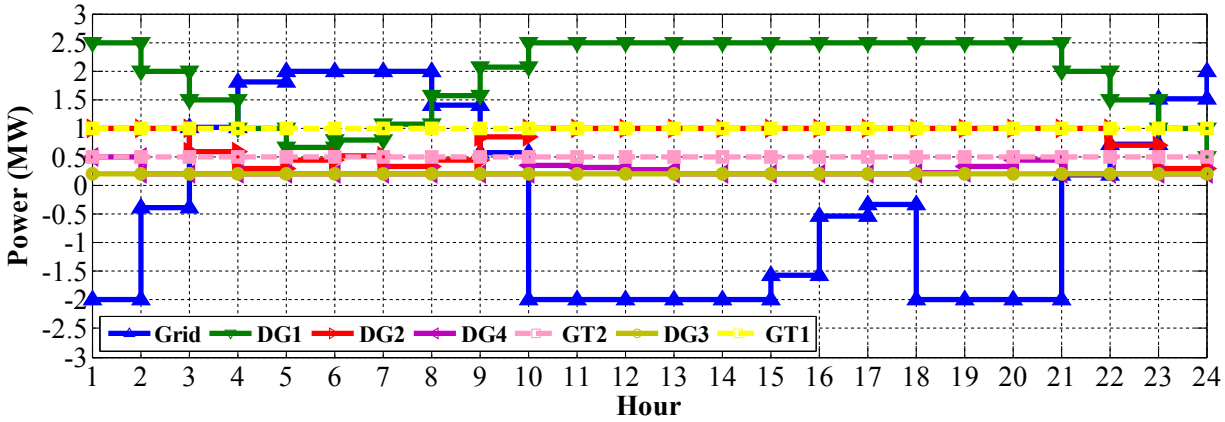

Fig.4. Active power of DGs and grid

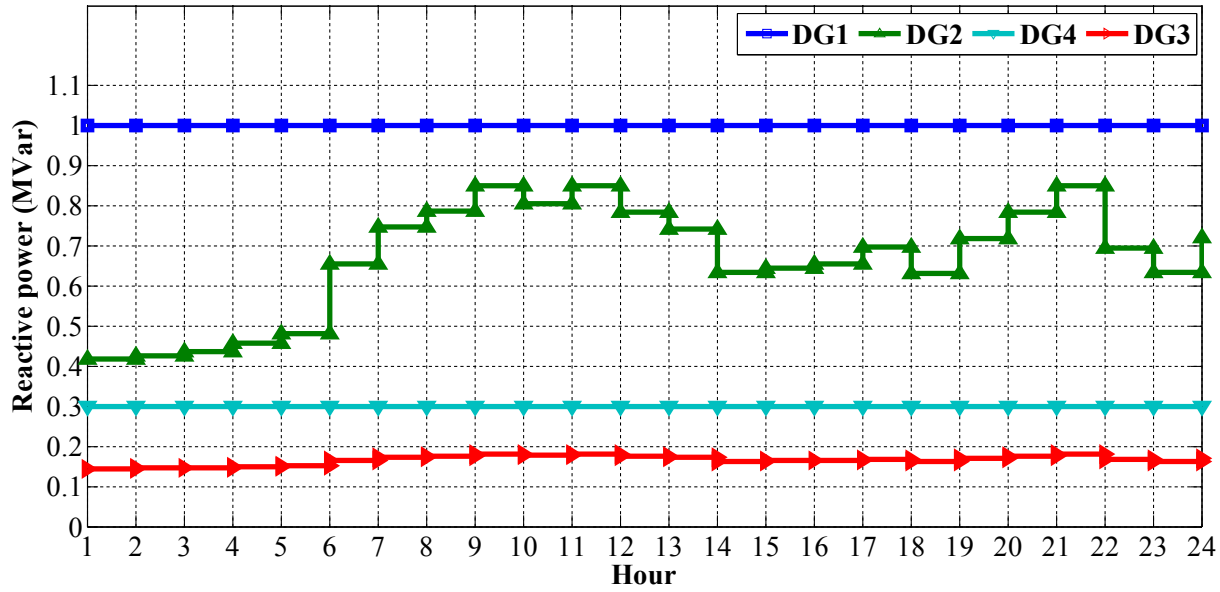

Fig.5. Reactive power of DGs

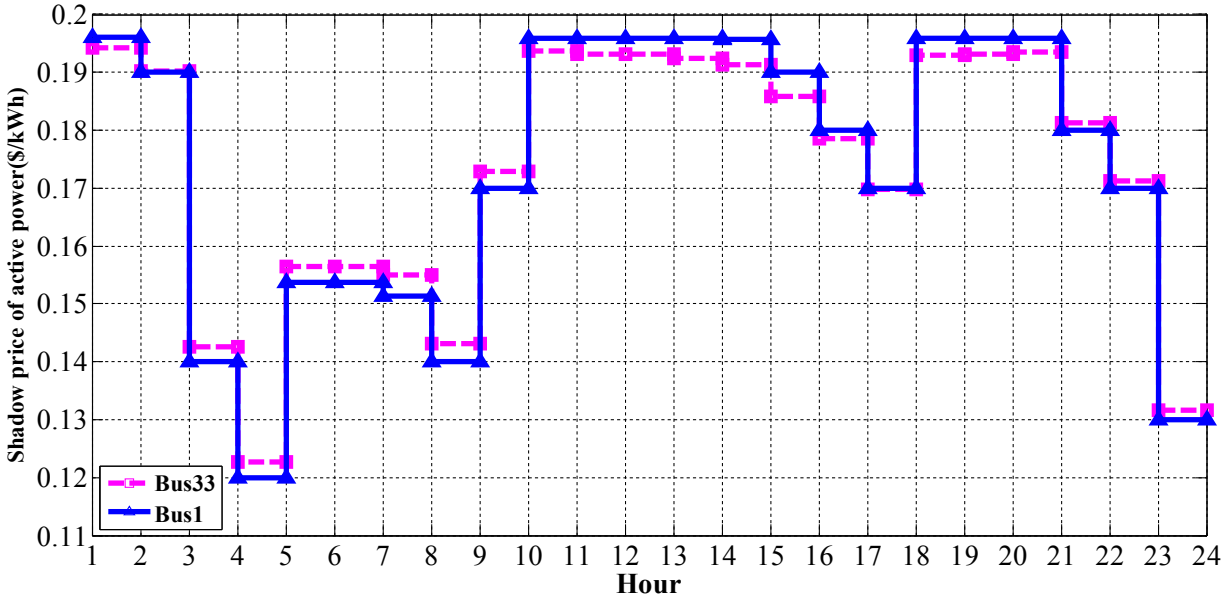

Fig.6. Shadow price of active power in the first and last buses of MG (in $/kWh) for different times

Now, in order to investigate the effect of the number of BSSs on MG operation cost, optimisation problem is solved for different number of BSSs and the results have been tabulated as Table 4. The results show that the number of BSSs does not significantly affect MG operation cost as the operation cost difference between using a single BSS and 25 BSSs is only 0.5%. It must be noted that in simulations, when the number of BSSs is increased, capacity of each BSS and maximum power are accordingly decreased.

Table 4. Results with higher number of BSSs

Number of BSSs	Capacity of each BSS	Maximum power	Optimal location	MG operation cost
1	30000	1.5	19	9689.4629
2	15000	0.75	2, 19	9688.0806
3	10000	0.5	2,11, 19	9697.6272
4	7500	0.375	1, 2, 11, 19	9691.3186
6	5000	0.25	1-3,11,19,20	9697.9372
7	4285.7143	0.2143	1-3,11,19-21	9702.2774
8	3750	0.1875	1-3,10,11,19-21	9704.7774
9	3333.3333	0.1667	1-4,10,11,19-21	9706.8309
10	3000	0.15	1-4,10,11,19-22	9709.4642
15	2000	0.1	1-5,10-12,19-23,27,31	9719.1707
20	1500	0.075	1-6,9-12,19-24,26,27,31,33	9730.4582
25	1200	0.06	1-13, 19-28, 31, 32	9740.1509

4.2. Sensitivity of MG operation cost with respect to BSS location, BSS size and BSS-MG power exchange limit

In this subsection, the sensitivity of MG operation cost with respect to BSS location, BSS size and BSS-MG power exchange limit are investigated. Table 5 shows MG operation cost when BSS is placed at different buses of the MG. The least MG operation cost happens when BSS is placed at bus 19 and the maximum MG operation cost occurs when BSS is placed at bus 18. The difference between the best and worst location in daily operation cost is 472.3422$, namely 4.9%. This indicates that selecting the best location for BSSs in MGs is important. Placing BSS at different buses leads to different power flows, different voltages, different losses and thereby different MG operation costs. Interesting point is that placing BSS at buses 18 and 19 which are close in the MG lead to very different operation costs.

Table 5. MG operation cost for different BSS locations

BSS location	Optimal MG operation cost ($)	BSS location	Optimal MG operation cost($)
1	9693.3449	18	10161.8051
2	9689.5924	**19**	**9689.4629**
3	9734.5527	20	9764.6517
4	9750.6620	21	9784.0287
5	9765.1864	22	9814.9323
6	9791.8708	23	9770.5661
7	9798.7682	24	9840.5291
8	9838.8358	25	9896.8448
9	9852.1763	26	9798.2041
10	9862.3796	27	9806.0274
11	9863.5672	28	9848.9431
12	9883.7208	29	9879.9269
13	9960.7087	30	9896.0883
14	9988.2480	31	9916.6841
15	10014.6271	32	9933.5871
16	10055.8989	33	9948.1480
17	10125.2135		

Table 6 shows optimal MG operation cost and optimal BSS location for different BSS sizes. In a certain region, the size of BSS of a certain EV model is chosen based on the daily demand of EVs of the same model. The interesting point is that optimal BSS location depends on its size. For sizes 7500 kWh, 93755 kWh, 11250 kWh, 13125 kWh and 15000 kWh, bus 1 is the best location for BSS, for sizes between 16875 kWh and 30000 kWh, bus 19 is the best BSS location. For size of 33750 kWh, bus 5 is optimal BSS location and for sizes 31875 kWh, 35625 kWh and 36000 kWh, bus 2 is the optimal location for BSS. The important point is that this MG cannot support BSS with more than 480 batteries or larger than 36000 kWh, as the model would be infeasible. As expected, MG operation cost increases with increase in BSS size. Fig.7 illustrates MG operation cost at different BSS locations.

Table 6. Optimal BSS location for different BSS size

Number of batteries	BSS size (kWh)	Optimal BSS location	Optimal MG operation cost ($)
100	7500	1	5841.5502
125	9375	1	6134.8797
150	11250	1	6430.9214
175	13125	1	6730.0379
200	15000	1	7032.3969
225	16875	19	7349.2759
250	18750	19	7667.5086
275	20625	19	7986.2717
300	22500	19	8306.6137
325	24375	19	8639.5777
350	26250	19	8977.3400
375	28125	19	9327.9150
400	300000	19	9689.4629
425	31875	2	10057.7812
450	33750	5	10503.1195
475	35625	2	10842.7689
480	36000	2	10928.8457
481	36075	NA	NA

Table 7 includes MG operation cost and optimal BSS location for different maximum power of BSS. With higher BSS maximum charging/discharging power, at low-price hours BSS is able to absorb higher power from cheap power resources and at high-price hours, it is able to further increase energy arbitrage capability of MG and reduce the need to load expensive thermal DGs. Therefore, higher values for BSS maximum power lead to lower MG operation cost. However, MG operation cost versus BSS maximum charging/discharging power curve saturates when BSS maximum charging/discharging power reaches 4 MW and an operation cost less than $9297.0883 is not achievable. By further increase in BSS maximum charging/discharging power, MG operation cost does not decrease as other constraints are binding. Fig.8 illustrates MG operation cost versus maximum charging/discharging power of BSS.

Table 7. MG operation cost for different BSS maximum power

BSS maximum power (MW)	Optimal BSS location	Optimal MG operation cost($)
1.25	6	9933.1853
1.5	19	9689.4629
1.75	2	9567.4151
2	19	9487.4034
2.25	2	9428.2699
2.5	2	9384.9766
2.75	2	9344.2184
3	19	9323.072
3.25	1	9307.481
3.50	1	9300.7443
3.75	1	9297.5938
4	1	9297.0883
4.5	1	9297.0883

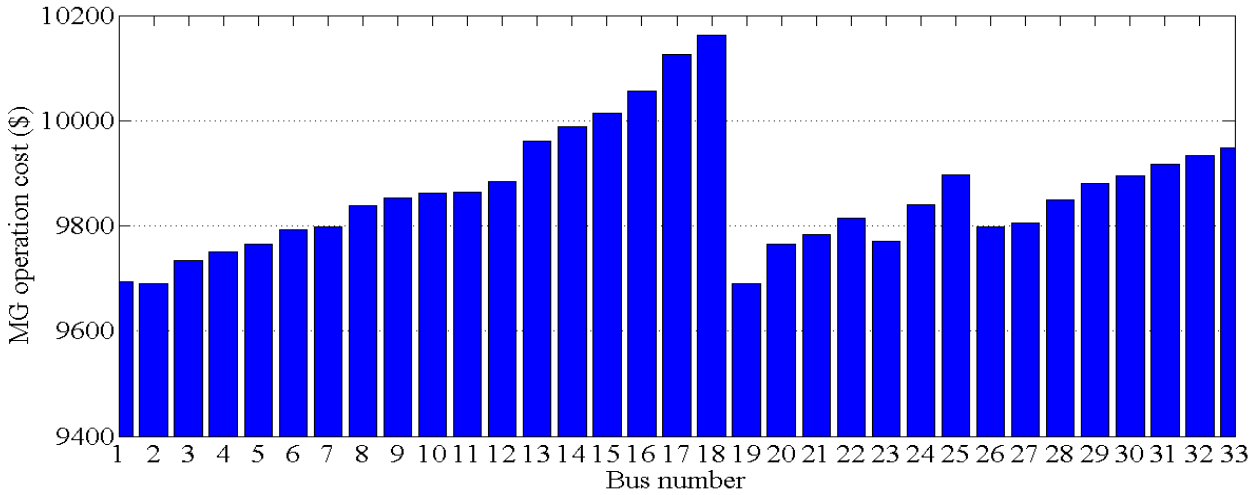

Fig.7. MG operation cost with different BSS location

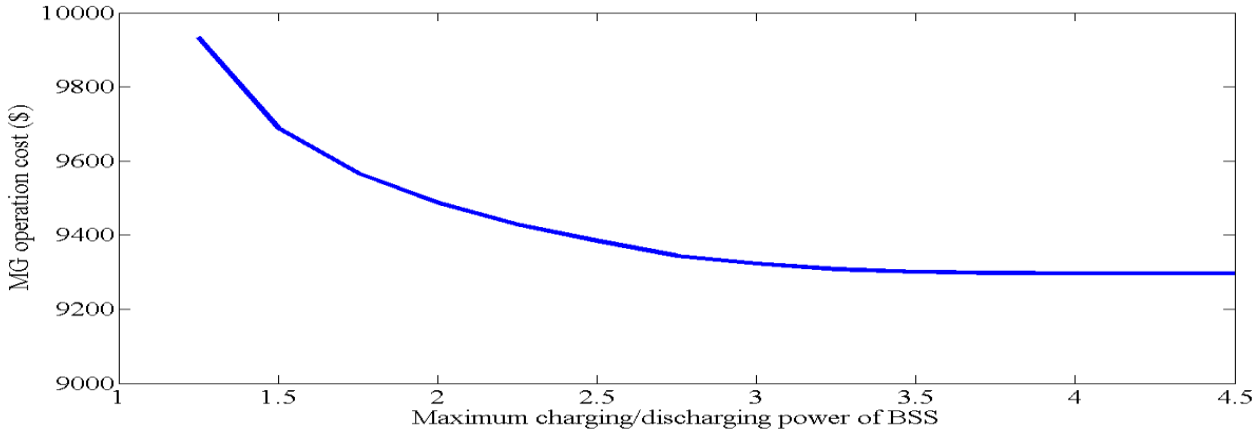

Fig.8. MG operation cost versus maximum power of BSS

4.3. Effect of PHS unit, PHS capacity and maximum PHS charging/discharging power on MG operation cost and optimal BSS location

In order to evaluate the effect of PHS unit on the operation of the MG, the model is solved without PHS unit. While, with PHS unit, MG operation cost was $9689.4629 and bus 19 was optimal BSS location, now without PHS unit, MG operation cost increases to $10056.1847 and bus 11 is optimal BSS location. This implies that integrating PHS unit into MG changes optimal location of BSS and decreases MG operation cost by 3.65%. Fig.9 contains dispatch of MG resources when PHS unit is not integrated in the MG. The role of PHS unit is to be charged in low-price hours when cheap grid power can be purchased and be discharged in high-price hours to prevent heavy loading of expensive thermal DGs and decrease MG operation cost. As an example, compare Fig.9 and Fig.4 for hour 10. At this hour, with PHS unit, DG4 as an expensive power resource generates only 0.3569 MW but without PHS unit, it generates 0.5 MW.

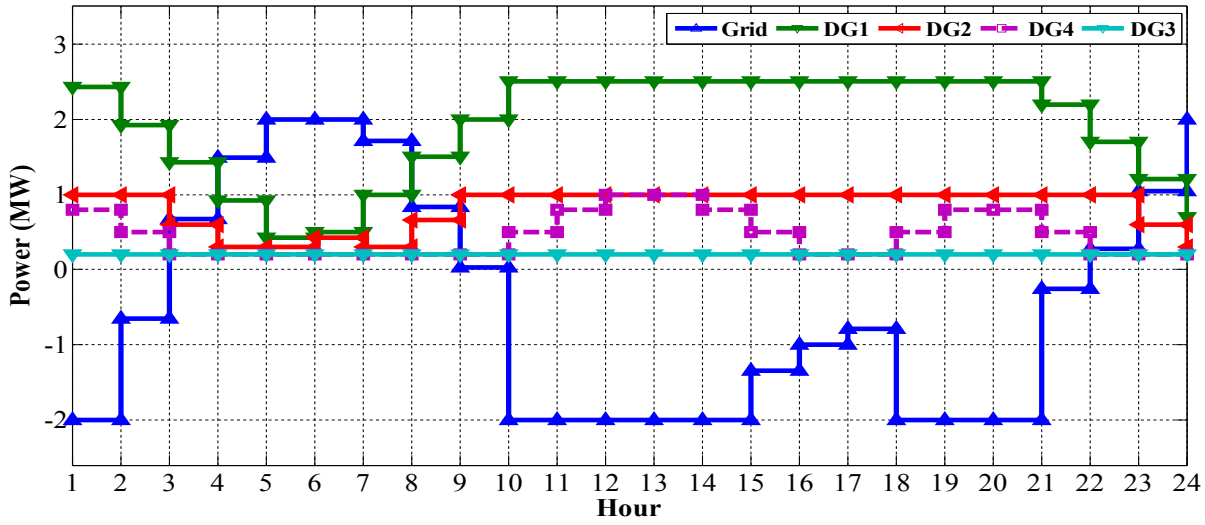

Fig.9. Active power of DGs and grid power without PHS unit

In order to investigate the effect of PHS capacity on MG operation, the model has been solved for PHS capacities ranged from 50 kWh to 6000 kWh. MG operation cost and optimal BSS location for different PHS capacities have been tabulated as Table 8 and Fig.10 illustrates MG operation cost versus PHS capacity. According to Table 8, optimal BSS location is not affected by PHS capacity, however, increasing PHS capacity decreases MG operation cost. The increase in PHS capacity enables it to store higher energy during low-price hours and inject higher power to MG during high-price hours; thereby energy arbitrage capability of MG increases and its operation cost decreases. By increase in PHS capacity, the slope of the curve decreases and it saturates. At PHS capacity of 4 MWh and above, the effect of increase in PHS capacity on MG operation cost is

negligible, because other constraints would be binding and would not allow further improvement in MG operation cost.

Table 8. MG operation cost for different PHS capacities

PHS capacity (kWh)	Optimal BSS location	Optimal MG operation cost ($)
50	19	9883.6033
100	19	9877.3682
200	19	9865.8785
300	19	9854.9588
400	19	9844.2473
500	19	9833.7265
1000	19	9792.0673
2000	19	9735.7929
3000	19	9698.0115
4000	19	9689.463
5000	19	9689.463
6000	19	9689.4629

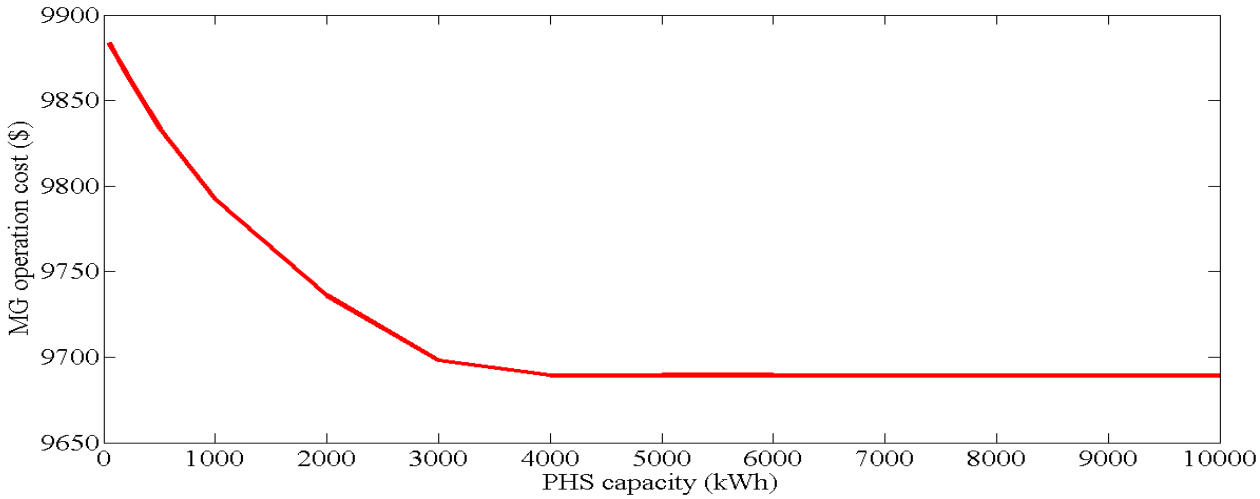

Fig.10. MG operation cost with different PHS capacities

Eventually, the effect of maximum charging/discharging power of PHS on MG operation has been investigated and the results have been tabulated as Table 9. The Table indicates that with increase in maximum charging/discharging power of PHS, MG operation cost decreases. This is due to the fact that by increase in its maximum charging/discharging power, PHS absorbs higher power and energy at low-price hours when cheap power resources are available and injects higher power to the MG during high-price hours and decreases loading of expensive DGs. With maximum charging/discharging power of 0.6 and higher, the model would be infeasible. Optimal BSS location is not affected by variations in maximum charging/discharging power of PHS.

Table 9. MG operation cost for different maximum charging/discharging power of PHS

PHS maximum charging/discharging power	Optimal BSS location	Optimal MG operation cost($)
0.05	19	9865.5790
0.1	19	9842.7569
0.15	19	9820.8276
0.2	19	9800.0764
0.3	19	9761.9074
0.4	19	9724.4128
0.5	19	9689.4629
0.6 and above	**Infeasible**	**Infeasible**

5. Conclusions

In this paper, optimal location of BSSs has been determined in MGs with PHS, photovoltaic, wind and geothermal units, while reactive power dispatch, DGs constraints and all network constraints are considered in AC optimal power flow. AC optimal power flow has been formulated as a mixed-integer nonlinear optimisation problem that the voltages of buses at different times, schedule of DGs, BSS and PHS unit, schedule of power exchange with grid, load shedding schedule and BSS location form decision vector. The effect of BSS capacity and maximum power, BSS to MG link capacity, PHS capacity and maximum charging/discharging power of PHS unit on MG operation and optimal BSS location have been investigated.

The results indicate that selecting the best location for BSSs is important, because the difference between the best and worst location in daily operation cost of MG is as high as 4.9%. The interesting point is that placing BSS at neighbor buses may lead to very different operation costs. The results also indicate that optimal BSS location depends on its size and its maximum charging power but does not depend on maximum charging/discharging power of PHS and PHS capacity.

Acknowledgements

There is no conflict of interest for this paper. J.P.S. Catalão acknowledges the support by FEDER funds through COMPETE 2020 and by Portuguese funds through FCT, under POCI-01-0145-FEDER-029803 (02/SAICT/2017).

References

[1] D.T. Ton, M.A. Smith, The US department of energy's microgrid initiative, The Electricity Journal, 25 (2012) 84-94.
[2] A.R. Jordehi, Dynamic environmental-economic load dispatch in grid-connected microgrids with demand response programs considering the uncertainties of demand, renewable generation and market price, International Journal of Numerical Modelling: Electronic Networks, Devices and Fields, (2020).
[3] A.R. Jordehi, Mixed binary-continuous particle swarm optimisation algorithm for unit commitment in microgrids considering uncertainties and emissions, International Transactions on Electrical Energy Systems, (2020).
[4] M.S.J. A. Rezaee Jordehi, João P. S. Catalão, Dynamic economic load dispatch in isolated microgrids with particle swarm optimisation considering demand response, in: IEEE UPEC, IEEE, Torino, Italy, 2020.
[5] H. Khaloie, A. Abdollahi, M. Shafie-Khah, P. Siano, S. Nojavan, A. Anvari-Moghaddam, J.P. Catalão, Co-optimized bidding strategy of an integrated wind-thermal-photovoltaic system in deregulated electricity market under uncertainties, Journal of Cleaner Production, 242 (2020) 118434.
[6] S.M. Hakimi, A. Hasankhani, M. Shafie-khah, J.P. Catalão, Optimal sizing and siting of smart microgrid components under high renewables penetration considering demand response, IET Renewable Power Generation, 13 (2019) 1809-1822.
[7] R.Á. Fernández, Method for assessing the environmental benefit of road transport electrification and its influence on greenhouse gas inventories, Journal of cleaner production, 218 (2019) 476-485.
[8] Global greenhouse gas emissions data, Available at https://www.epa.gov/ghgemissions/global-greenhouse-gas-emissions-data, in.
[9] J.M. Islas-Samperio, F. Manzini, G.K. Grande-Acosta, Toward a Low-Carbon Transport Sector in Mexico, Energies, 13 (2020) 84.
[10] M.S.J. A. Rezaee Jordehi , João P. S. Catalão, Energy Management in Microgrids with Battery Swap Stations and Var Compensators, Journal of Cleaner Production, (2020).
[11] M. Mahoor, Z.S. Hosseini, A. Khodaei, Least-cost operation of a battery swapping station with random customer requests, Energy, 172 (2019) 913-921.
[12] Y. Zheng, Z.Y. Dong, Y. Xu, K. Meng, J.H. Zhao, J. Qiu, Electric vehicle battery charging/swap stations in distribution systems: comparison study and optimal planning, IEEE transactions on Power Systems, 29 (2013) 221-229.
[13] U. Sultana, A.B. Khairuddin, B. Sultana, N. Rasheed, S.H. Qazi, N.R. Malik, Placement and sizing of multiple distributed generation and battery swapping stations using grasshopper optimizer algorithm, Energy, 165 (2018) 408-421.
[14] J. Yang, H. Sun, Battery swap station location-routing problem with capacitated electric vehicles, Computers & Operations Research, 55 (2015) 217-232.
[15] I.E. Grossmann, J. Viswanathan, A. Vecchietti, R. Raman, E. Kalvelagen, GAMS/DICOPT: A discrete continuous optimization package, GAMS Corporation Inc, 37 (2002) 55.
[16] A. Soroudi, Power system optimization modeling in GAMS, Springer, 2017.
[17] Q. Tu, R. Betz, J. Mo, Y. Fan, Y. Liu, Achieving grid parity of wind power in China–Present levelized cost of electricity and future evolution, Applied Energy, 250 (2019) 1053-1064.
[18] A. Orioli, A. Di Gangi, Six-years-long effects of the Italian policies for photovoltaics on the grid parity of grid-connected photovoltaic systems installed in urban contexts, Energy, 130 (2017) 55-75.
[19] B. Guezuraga, R. Zauner, W. Pölz, Life cycle assessment of two different 2 MW class wind turbines, Renewable Energy, 37 (2012) 37-44.
[20] W. Luo, Y.S. Khoo, A. Kumar, J.S.C. Low, Y. Li, Y.S. Tan, Y. Wang, A.G. Aberle, S. Ramakrishna, A comparative life-cycle assessment of photovoltaic electricity generation in Singapore by multicrystalline silicon technologies, Solar Energy Materials and Solar Cells, 174 (2018) 157-162.
[21] J.W. Lund, T.L. Boyd, Direct utilization of geothermal energy 2015 worldwide review, Geothermics, 60 (2016) 66-93.
[22] L. Xia, Y. Zhang, An overview of world geothermal power generation and a case study on China—The resource and market perspective, Renewable and Sustainable Energy Reviews, 112 (2019) 411-423.

[23] N. Spittler, B. Davidsdottir, E. Shafiei, J. Leaver, E.I. Asgeirsson, H. Stefansson, The role of geothermal resources in sustainable power system planning in Iceland, Renewable Energy, (2020).
[24] L. Rybach, Geothermal sustainability, GHC Bulletin, September, (2007).
[25] Moomaw, W., P. Burgherr, G. Heath, M. Lenzen, J. Nyboer, A. Verbruggen, Annex II: Methodology. In IPCC: Special Report on Renewable Energy Sources and Climate Change Mitigation, in.
[26] W. Craig, K. Gavin, ICE Themes Geothermal Energy, Heat Exchange Systems and Energy Piles, ICE Publishing, 2018.
[27] M.S. Javadi, K. Firuzi, M. Rezanejad, M. Lotfi, M. Gough, J.P. Catalão, Optimal Sizing and Siting of Electrical Energy Storage Devices for Smart Grids Considering Time-of-Use Programs, in: IECON 2019-45th Annual Conference of the IEEE Industrial Electronics Society, IEEE, 2019, pp. 4157-4162.
[28] M.S. Javadi, M. Lotfi, M. Gough, A.E. Nezhad, S.F. Santos, J.P. Catalao, Optimal Spinning Reserve Allocation in Presence of Electrical Storage and Renewable Energy Sources, in: 2019 IEEE International Conference on Environment and Electrical Engineering and 2019 IEEE Industrial and Commercial Power Systems Europe (EEEIC/I&CPS Europe), IEEE, 2019, pp. 1-6.
[29] B. Steffen, Prospects for pumped-hydro storage in Germany, Energy Policy, 45 (2012) 420-429.
[30] D. Shirmohammadi, H.W. Hong, Reconfiguration of electric distribution networks for resistive line losses reduction, IEEE Transactions on Power Delivery, 4 (1989) 1492-1498.
[31] A. Khodaei, Microgrid optimal scheduling with multi-period islanding constraints, IEEE Transactions on Power Systems, 29 (2013) 1383-1392.
[32] A. Rezaee Jordehi, Particle swarm optimisation with opposition learning-based strategy: An efficient optimisation algorithm for day-ahead scheduling and reconfiguration in active distribution systems, Soft computing, (2020).
[33] A. Kavousi-Fard, A. Zare, A. Khodaei, Effective dynamic scheduling of reconfigurable microgrids, IEEE Transactions on Power Systems, 33 (2018) 5519-5530.